JOURNAL OF MATERIALS SCIENCE 14 (1979) 509–534

Review
Quantitative fractography

J. L. CHERMANT, M. COSTER
Laboratoire de Cristallographie et Chimie du Solide, L. A. No. 251, Equipe Matériaux–Microstructure, ISMRA–Université de Caen, 14032 Caen Cedex, France

In many disciplines, such as biology, botany, geology, materials science and medicine, quantitative image analysis is being used to an increasing extent. In materials science this technique makes it possible to relate the microsctructure to the mechanical properties. In this review we shall show that image analysis can be applied in a fractographic study to characterize quantitatively the morphology of fracture. Such an analysis provides information which, together with that obtained by mechanical tests, enables an explanation of the mechanism of rupture to be made.

The different problems encountered in quantitative fractography – analysis of fracture paths or of fractured surfaces – are presented, and the concept of mean plane of fracture is introduced. Whatever the type of analysis used, a small number of parameters exist which can be used to determine the size and proportion present of the different fracture morphologies. Then the stereometric relationships, first established for plane sections, are modified as a function of the morphology of the fracture surface. Methods based on the notion of linear roughness and on fractal object allow a quantitative description of the morphology of the fracture paths. A criticism is also made of the different types of analysis – manual, semi-automatic and automatic – used in quantitative fractography. Finally, some examples are given to show what kinds of investigations are possible using quantitative fractography.

Nomenclature

Geometric parameters

A	area (plane)
A'	projected area
$D(i)$	diameter of equivalent sphere of class i
$d(i)$	diameter of equivalent circle of class i
H	distance between two planes, tangent to a given object
L	length
L'	projected length
L_2	mean chord in space R2
L_3	mean chord in space R3
L_P	perimeter
k	curvature
a	major axis of ellipsoid of revolution
b	small axis of ellipsoid of revolution
ϵ	eccentricity of ellipsoid of revolution
t	thickness of the thin film analysed

Specific parameters

P_P	fraction of points
P'_P	fraction of projected points
V_V	volume fraction
N_V	number of objects per unit volume
L_V	length per unit volume
S_V	(curved) surface per unit volume
P_A	number of points per unit area
N_A	number of objects per unit area
N'_A	number of projected object per unit area
A_A	areal fraction
A'_A	fraction of projected surface
L_A	length per unit area
L'_A	projected length per unit area
N_L	number of objects per unit length
N'_L	number of objects per unit projected length
L_L	fraction of length
L'_L	fraction of projected length

L_S length per unit of curved surface
N_S number of objects per unit curved surface
S_S fraction of curved surface

Parameters of quantitative fractography itself

K fraction of fracture nominally flat
E thickness of plastic zone
R_L linear roughness index, according to Pickens and Gurland
P_S waveiness or linear index, according to Chermant, Coster and Osterstock
Δ discrepancy parameter at rupture
ρ ratio of value measured on fracture surface to those measured on a polished surface
D_c critical diameter

Other parameters

$L_{(j)}$ Saltykov coefficient
X geometrical set to be analysed
x position of the structuring element
h measurement step size
r size of the structuring element
h' projection of step of size h
B structuring element
$\gamma(h)$ variogram function
$\mathscr{E}$ mathematical probability
$\mathscr{D}$ fractal dimension
σ_{rf} rupture stress in bending
$\bar{L}_{Co}$ mean free path in the cobalt phase
$\bar{D}_{WC}$ mean diameter of tungsten carbide crystals
K_{IC} critical stress intensity factor

1. Introduction

For a number of years, the mechanical properties of materials have been studied with ever greater accuracy. The progress made in the field of fracture mechanics has enabled a better understanding of the behaviour of these materials to rupture. Nevertheless the theoretical models proposed and the experimental results are not always sufficient to enable a correct interpretation of the results if the morphology and features of fracture are not known sufficiently well, if that is quantitatively possible.

It is possible at the present time to describe quantitatively, quite satisfactorily, the morphology of the majority of materials, either from a surface analysis or analysis of thin films. The methods are described in general publications [1–3]. A new concept of image analysis has developed over the last few years, based on principles of mathematical morphology [4–6]. This new concept considerably enriches the potential of image analysis.

On the other hand the literature on quantitative analysis of rupture surfaces is much more limited. Apart from the theoretical work of El Soudani [7], Coster [8], Chermant *et al.* [9], and some works on the study of fracture of materials, there has been little published in this field. One reason for this is certainly the fact that it is impossible to analyse a fractograph with automatic instruments. In spite of these difficulties quantitative fractography should be developed because it permits a comparison of the morphology of a material with that of fracture, and thus complements the information that can be obtained by fracture mechanics.

2. Methods of observation

When a material is fractured it is possible to study the fracture surface or, in the case of plate specimens, the intersection of the fracture surface with the specimen surface. This is termed the "line of fracture" or fracture path.

In the majority of cases the fracture surface is non-planar. It is therefore necessary that the method of observation chosen has a depth of focus sufficient for all points of the fracture surface to be in focus (focusing screen of the microscope, TV screen, photographic plate). Hence it is scarcely possible to use optical microscopy. On the other hand, if low magnifications are used, one could employ macrophotographical techniques. For higher magnifications, electron microscope replica studies can be used or scanning electron microscopy on the surface observed directly.

The preparation of replicas can prove difficult as it may be impossible to extract the replica properly from certain areas. In scanning electron microscopy these difficulties do not exist since the specimen itself is introduced into the microscope.

In both cases there exists the problem of the direction of observation relative to the fracture surface. This problem will be discussed in the following paragraph; first, certain concepts must be introduced in order to determine the most favourable direction of observation.

The problem of sampling of the replica has been resolved for composite materials of the type WC–Co [8,9] as a comparison of the size distribution measured on replicas and that measured on a scanning electron microscope for the same

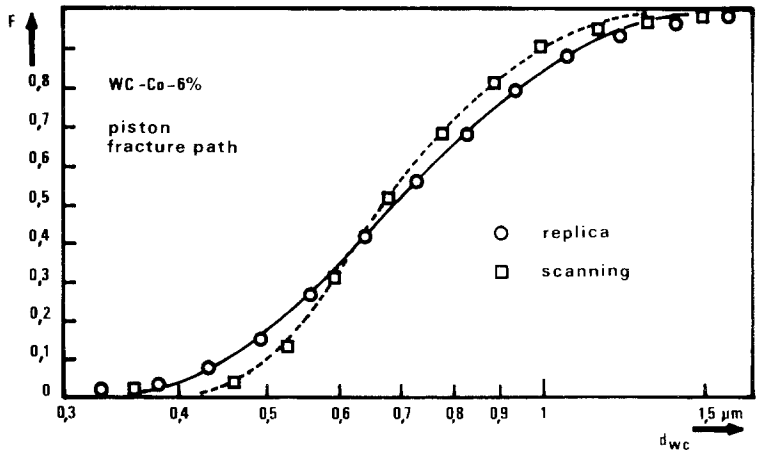

Figure 1 Comparison of distribution curves for WC crystals in a fracture surface of a WC–Co anvil, with Co 6 wt%, in the scanning electron microscope and by replica.

material. Fig. 1 shows that the size distribution curves of WC on the fracture surface of a WC–6 wt% Co for the two methods are very similar, and that the difference between the two is less than the errors in the measuring methods (analysis made semi-automatically with a Zeiss Analyser TGZ 3). This result demonstrates that no falsification in the results takes place during extraction of the replica. This does not imply that for other specimens falsification does not arise. It is necessary therefore to verify this for each material.

Apart from the difficulties of replica sampling, scanning electron microscopy offers other advantages, in particular with suitable accessories it is possible to obtain X-ray images of the fracture, which give complementary information regarding the distribution of different atomic elements on the fracture surface. This problem will be discussed again in the critical review of measurable parameters.

When the fracture line is observed in a parallelepiped specimen, the line of fracture lies in the plane of the specimen if the plastic deformation before fracture is not too large, e.g. brittle materials (in this case the outer fibre is always considered as plane). Otherwise the quantitative fracture analysis is very difficult. It is thus possible in these brittle materials to use optical microscopy at least for moderate magnifications. On the other hand if larger magnifications are necessary or if appreciable deformation occurred before fracture, it is preferable to use a scanning electron microscope.

3. Problems in the analysis of fracture surfaces

As mentioned in the previous paragraph, a fracture surface is generally not planar and if this presents problems in observation, the same applies to the quantitative analysis of the microstructural feature of fracture. The first problem to be resolved is what direction of observation should be employed to make a quantitative fractographic analysis? Before an answer can be given, it is necessary to examine quantitatively the rupture surface morphologies which could arise.

3.1. Classification of fracture surfaces

El Soudani in his theoretical article has proposed a classification [7]. He introduced first the concept of a surface intersecting the fracture surface such that the volume of the solid above the dividing surface is equal to the total volume of hollows below it. Based on this dividing surface, he has defined several possible morphlogies (Fig. 2).

(a) *Ideally flat fracture surface,* with coincides at all points with its dividing plane.

(b) *Nominally flat fracture surface,* in which the dividing surface is planar.

(c) *Random-curvature fracture surface,* in which the surface normal can assume any direction.

(d) *Stepped fracture surface,* often observed in cases of brittle fracture.

(e) *Zigzagging fracture surface,* observed, for example, in the case of complex states of stress at the crack tip or when more than one mode of fracture is operative.

(f) *Complex fracture surface,* which is a combination of the above types.

This classification is interesting, but the classification of an actual fracture surface is a question of magnification. For example, a fracture surface could appear to be nominally flat at low magnifications and yet at higher magnifications appears random (see for example a razor blade). As El Soudani also indicated, it is necessary to specify

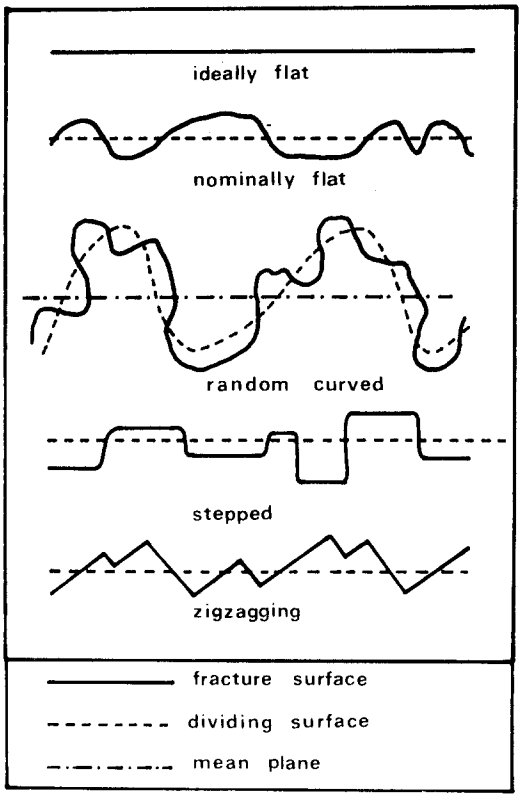

Figure 2 Morphology of the various fracture features, after El Soudani.

the magnification at which the classification was made. Fig. 2 shows the position of the mean surface with respect to the fracture surface.

3.2. Choice of direction of observation

If we assume that the direction of observation ought to be perpendicular to the surface, this is uniquely defined if the surface is flat (always the case in metallography). In fractography, however, an ideally flat surface is virtually never observed. In the various morphologies defined by El Soudani it can be seen that the dividing surface is flat for the case of nominally flat fracture surfaces, stepped fracture surfaces and zigzagging fracture surfaces. For these three types one could take as the observation direction the normal to the planar dividing surface. In random fracture surfaces or complex fracture surfaces the concept of the dividing surface is insufficient as far as defining the direction of observation is concerned, It is necessary to introduce the concept of a mean plane defined as a plane cutting the dividing surface such that the volumes above and below the mean plane are equal. This mean plane is hence an extension of the concept of the dividing surface proposed initially. Thus the direction of observation can always be defined as the normal to the mean fracture plane, irrespective of the morphology of fracture.

The practical problem for the experimenter is to determine as accurately as possible this mean fracture plane. We shall see that the solution to this problem depends upon the means of observation—transmission electron microscope or scanning electron microscope. In transmission electron microscopy, a replica is examined, which is supported on a grid. The replica always sags and the projection of the surfaces always lies in the plane of the grid. Therefore as far as fractography is concerned the direction of observation is imposed by the apparatus, being normal to the grid. It will be seen that the mean fracture plane is in the zone virtually always considered parallel to the grid. In the scanning electron microscope, where one observes the fracture directly, it is necessary to apply certain rules to choose the direction of observation. The recommended method is the following (i) the fracture surface is observed under the lowest available magnification (or at a magnification such that the whole fracture surface appears on the cathode ray screen), (ii) the specimen is oriented such that the fracture surface exhibits the least possible relief; the recommended direction of observation is thus defined.

3.3. Validity and limits of the laws of stereology: stereometric relations

The morphological characteristics of materials are defined in three dimensional space. Stereology attempts to establish relationships between the results obtained in a two dimensional analysis (R2) and the true three-dimensional microstructural parameters [3]. The stereometric relationships depend on the mode of observation: they have been established for measurements on an image obtained by reflection of a planar section, whereas the image in transmission is the projected image of objects contained in a thin film.

The measurable parameters in these two examples are of two types. Firstly here are parameters which correspond to mean values and secondly parameters which correspond to distributions. These parameters depend on the method of observation.

TABLE I General relationships in stereology for the case of a section

Unknown quantities in R3 space		Volume, V_V	Surface, S_V	Length, L_V	Number, N_V
Quantities measurable in R2 space	Surface, A	Fraction of area occupied, A_A	Length of line per unit area L_A	Number of points per unit area, P_A	Number of objects per unit area, N_A
	Length, L	Fraction of line occupied, L_L	Number of intersections per unit length, N_L		
	Points, P	Fraction of points P_P			
Stereometric relationships		$\bar{P}_P = \bar{L}_L = \bar{A}_A = \bar{V}_V$ $\bar{L}_2 = \bar{L}_3 = \frac{\bar{V}_V}{\bar{N}_L}$	$\bar{L}_A = \frac{\pi}{2}\bar{N}_L$* $\bar{S}_V = \frac{4}{\pi}\bar{L}_A$ $\bar{S}_V = 2\bar{N}_L$*	$\bar{L}_V = 2\bar{P}_A$	$\bar{N}_A = \bar{N}_V\bar{D}_V$

*As defined according to Underwood.

TABLE II General relationships in stereology for a thin film analysed in projection.

Unknown quantities in R3 space		Volume, V_V	Surface S_V	Length L_V	Number, N_V
Quantities measurable in R_2 space	Surface, A		Projected surface, A'_A	Perimeter of projection per unit surface, L'_A	Number of projected objects per unit surface, N'_A
	Length, L			Fraction of projected chord, L'_L	Number of projected objects per unit length, N'_L
	Point, P				Fraction of projected points, P'_P
Stereometric relationships		$\bar{V}_V = \bar{A}'_A\bar{L}_3/t$	$\bar{S}_V = 4\frac{\bar{A}'_A}{t}$	$\bar{L}_V = \frac{4}{\pi}\frac{\bar{L}'_A}{t}$ $\bar{L}_A = \frac{\pi}{2}\bar{L}'_A$	$\bar{N}_V = \bar{N}'_A/t$ $\bar{N}'_A = \bar{N}'_A = \bar{N}'_L/t$ $\bar{P}_L = \bar{P}'_P/t$

Tables I and II show the principal parameters measuring mean values either from analysis of a section or a thin film. Obviously other parameters can be derived by combined principal parameters. The tables give a general overview of the relationships between measurable quantities and the quantities contained in the volume. It can be seen that the transition from n to $(n + 1)$ dimensions is made only vertically in each column. Thus it is evident that N_V is a quantity inaccessible to section analysis, whereas V_V is inaccessible to thin film analysis. To obtain these quantities it is necessary to make a hypothesis and construct a model.

3.4. Application of stereometric analysis of a fracture surface without preconceived hypothesis

In the case of analysis of fracture surface, the image is no longer planar and the laws established for sections have to be revised. In general terms the laws we shall present or derive are valid for random fracture lines, but without any re-entrant parts.

El Soudani first showed that for such fracture types the fraction of surface occupied by an object or a type of fracture is equal to the areal fraction, fraction of line or points, measured on the projected image:

$$S_S = A'_A = L'_L = P'_P \qquad (1)$$

where S_S is the fraction of surface occupied by the phase or type of fracture,

A'_A is the areal fraction of the projected image,

L'_L is the lineal fraction of the normal image,

P'_P is the point fraction of the projected image.

This law thus enables one to calculate the proportion of brittle or ductile fracture, or the proportion of transgranular or intergranular fracture, if the limits are distinguishable in the image.

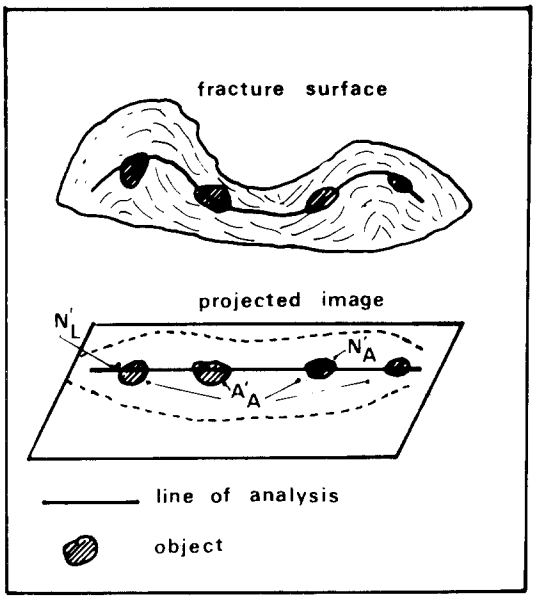

Figure 3 Parameters measured on projected images.

This type of relationship is valid for both nominally flat and random fracture surfaces.

It is known that the image projected on to the mean plane of fracture does not give directly the actual dimensions of the features (surface area or length). It is thus not possible to establish from these images the fracture characteristics per unit length or unit surface, using the relationships derived for plane sections. On the other hand some relationships established for projected images can be applied in the case of fracture surfaces, under certain conditions (Fig. 3).

If a random fracture surface, without re-entrant or overlapping curvatures, is considered, the same situation arises when analysing an open surface by projection. Kendall and Moran [10] have shown that an open surface of this type has an area double that of its image obtained by projection:

$$S = 2A' \tag{2}$$

This relationship was also established by El Soudani [7].

Still considering Fig. 3, a line "L" traced on the surface is projected on to the plane of analysis as a line "L'". Since the orientation is random, the line randomly traced on the surface is likewise random in the volume which contains this surface. For this case Underwood has shown that [3]:

$$L = \frac{4}{\pi} L' \tag{3}$$

The number of intersections or objects per unit length can thus be calculated. If there are N objects, then:

$$N_L = \frac{N}{L} = N \frac{\pi}{4} \frac{1}{L'} = \frac{\pi}{4} N'_L \tag{4}$$

If this random fracture surface contains characteristic features (intersections of grain surface with fracture surface, rivers patterns in the case of brittle fracture), it is thus possible to calculate the length of these fractures per unit area of fracture surface. One obtains from Equations 2 and 3:

$$\frac{L}{S} = \frac{4}{\pi} L' \frac{1}{2A'} = \frac{2}{\pi} \frac{L'}{A'}$$

from where:

$$L_S = \frac{2}{\pi} L'_A \tag{5}$$

Similarly the number of features per unit fracture surface can be deduced from Equation 2, if the number of particles per unit projected area, N'_A, is known:

$$N_S = \frac{N'_A}{2} \tag{6}$$

The mean length of these features can be calculated from a linear analysis. For a plane surface:

$$L_2 = \frac{V_V}{N_L} = \frac{A_A}{N_L}$$

In the case of a fracture surface therefore:

$$L_2 = \frac{S_S}{N_L} = \frac{4}{\pi} \frac{A'_A}{N'_L} \tag{7}$$

We have thus established the majority of the stereometric relationships defining the mean quantities on a random fracture surface. It is also interesting to know, for example, the distribution of particle size appearing in the fracture surface. Here there is the problem of the method of measurement, especially in the case of intergranular fracture. In an intergranular fracture, the fracture more or less skirts the grain (Fig. 4); the fracture surface and the enclosed surface determine a closed line of which the projection is only seen. Knowing the size of the enclosed line it can be reasoned that it is contained in a mean secant plane. Granulometry analysis consists therefore, in measuring

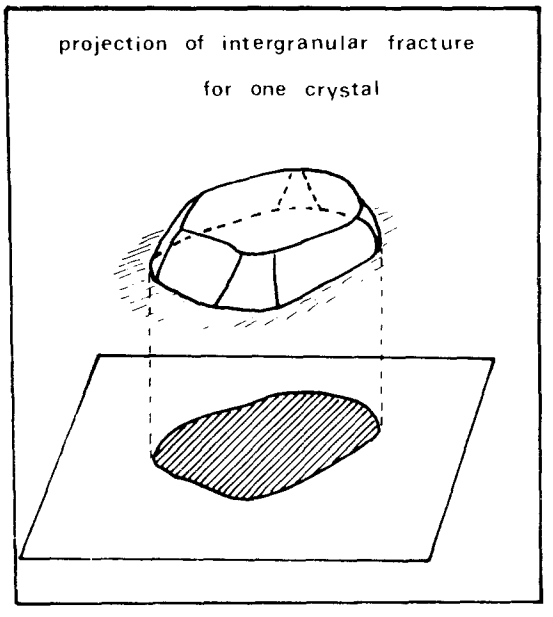

Figure 4 Projection of an intergranular fracture.

the size of the area enclosed by the closed curve, and this is particularly useful in the case of intergranular fracture. As in the case of quantitative metallography, one has the choice between surface analysis and linear analysis. The classification can be made of either the projected area or the chord length obtained by intersection of an analysis line and the projected image. Measurement is made according to a method comparable to that for a section, and the true value of the chord length or area is obtained using stereometric relationships.

In the case of measurement of traverses, the relationship existing between a line contained in a randomly oriented plane and its projection has been given by Kendall and Moran [10] as:

$$L = \frac{\pi}{2} L'.$$

Therefore all the distributions of traverses are translated by a factor $\pi/2$ on the abscissa.

For granulometric measures using the areal method, it can be shown similarly that:

$$A' = \frac{2A}{\pi} \int_0^{\pi/2} \cos\theta \, d\theta$$

$$A' = \frac{2A}{\pi}$$

from where:

$$A = \frac{\pi}{2} A' \tag{9}$$

Likewise it is observed that all areal distributions are translated by $\pi/2$.

All the equations, as we shall show, are valid solely for random fracture. In nominally plane fracture Relationship 1 remains valid, but on the other hand Relationship 2 is no longer valid as the fracture surface has a preferred orientation parallel to the plane of observation [7]:

$$A < S < 2A \tag{10}$$

The same applies for all the other quantities calculated above, as can be seen in Table III. It should be noted that for an ideally flat fracture surface, all the relationships derived for sections are valid. They are summarized in Table III. It can be seen that for a nominally flat fracture surface the parameters are included between those for an ideally flat fracture and a random fracture surface. The calculation of these parameters are assumed for a nominally flat fracture surface only if assumptions as to the morphology of the fracture are made.

TABLE III Stereologic relationships for fracture surfaces

Type of fracture surface	Ideally flat	Nominally flat	Random
S_S	$A'_A = L'_L = P'_P$	$A'_A = L'_L = P'_P$	$A'_A = L'_L = P'_P$
S	A'	$(2-K)A'$	$2A'$
L	L'	$\frac{K(\pi-4)+4}{\pi} L'$	$\frac{4}{\pi} L'$
N_S	N'_A	$\frac{K+1}{2} N'_A$	$\frac{N'_A}{2}$
N_L	N'_L	$\frac{K(4-\pi)+\pi}{4} N'_L$	$\frac{\pi}{4} N'_L$
L_S	L'_A	$\frac{K(\pi-2)+2}{\pi} L'_A$	$\frac{2}{\pi} L'_A$

The results obtained for different morphologies are only valid if it is assumed that the fracture surface is a homogeneous function of three-dimensional space (R3) [11]: strictly this case is never realized in practice, but it is assumed as a first approximation.

The comments regarding the first three fracture morphologies are no longer strictly valid for stepped or zigzagged fracture surfaces.

3.5. Extension of stereometric relationships to fracture surfaces, with hypotheses on the morphology

As we have seen, there are a numerous cases where quantitative analysis is scarcely possible without a preconceived hypothesis.

3.5.1. Quasi-ideally flat fracture surface

It can be assumed that a macroscopically flat fracture surface will remain so at the microscopic scale if the roughness is of the same order as the grain size or particles composing the material, if these are sufficiently small. This is the case for brittle fracture of a large number of ceramic materials or refractory carbides.

3.5.2. Nominally flat fracture surface

In order to calculate the parameters defining a nominally flat fracture surface, it is necessary to assume that this type of fracture can be subdivided into two other types:

(a) an ideally flat fracture surface which would have the same dividing surface;

(b) a random fracture surface.

If the proportion of each type is known, it is possible to calculate the parameters defined above. To obtain this proportion it is necessary to know the average profile of the fracture. Since the methods are the same as those used to analyse the line of fracture, we shall discuss them together.

In a nominally flat fracture surface a certain proportion corresponds to an ideally flat fracture surface. If K is this fraction, then the fraction of random fracture is $(1-K)$. The profile of such a fracture of length L and projection L' is calculated from the expression:

$$L = KL' + (1-K)\frac{4}{\pi}L'$$

from which is obtained:

$$K = \frac{\pi L - 4L'}{(\pi - 4)L'} \tag{11}$$

K can thus be calculated after measuring the profile and its projection. Knowing K, it is possible to calculate the other expressions listed in Table III.

3.5.3. Stepped or zigzagging fracture surface

Unlike the previous cases, the calculations are not valid when the fracture surface is not random. Each type of fracture corresponding to this calculation must be studied individually either by subdividing the surface to obtain one of the classifications described above or by making some assumption as to the morphology. In particular, the stepped fracture could be considered as a flat fracture, and the analysis of the profile would provide information on the step height.

3.6. Examples of stereological models applicable to fractography

We have shown that as a result of certain precautions and possibly corrections, it is possible to obtain the surface distribution of particle sizes seen in the fracture. It can be interesting to know the size distribution not in the surface but expressed by a parameter defining the true size of the particles. A critical study of some correction methods has already been described [9]. The Saltykov correction method [1] offers the advantage on the one hand of a logarithmic distribution of classes (the numerous size distribution curves approximate in effect a logarithmic distribution law) and on the other hand of being less sensitive to non-sphericity of particles than the methods using linear analysis. In the Saltykov method one calculates first the probability with which spheres of size (i) are cut by a random plane according to a circle which belong to the class $(i-j)$. This probability is such that the areal fraction occupied by the class $(i-j)$ is proportional to the areal fraction occupied by class (i). Saltykov have shown that this coefficient of proportionality does not depend on the separation between classes (i) and $(i-j)$, i.e. depends only on (j). This is a consequence of the choice of the geometric progression for the classes. The coefficients are called L_j. Thus knowing the distribution of equivalent circles, one can calculate the distribution of the diameters of the equivalent sphere from the number of

particles per unit volume using the equation:

$$N_V(i) = \frac{[d^2(i)N(i)/\Sigma d^2(i)N(i)]\,[V_V/L(o)][1 - \frac{1}{6}\pi \sum_{j=1}^{k-i} L(j)N_V(i+j)D^3(i+j)]}{\frac{1}{6}\pi D^3(i)} \quad (12)$$

where

- $d(i)$ is the diameter of equivalent circle of class (i),
- $D(i)$ is the diameter of equivalent sphere of class (i),
- $L(j)$ are the Saltykov coefficients,
- $N_V(i)$ is the number of particles per unit volume,
- V_V is the volume fraction of particles.

Using similar reasoning as Saltykov, we have derived [8] an expression to calculate the distribution of number of particles per unit surface, having a given diameter of equivalent sphere. The expression relating N_V and N_A is thus:

$$N_A(i) = \frac{2}{3} N_V(i) D^3(i) \left[\frac{1}{D^2(i)} + \frac{1}{L(o)} \sum_{j=1}^{j=i} \frac{L(j)}{D^2(i-j)}\right]. \quad (13)$$

This expression can be applied to fracture surfaces assuming that each particle is cut randomly in the case of transgranular fracture, or that the average fracture plane intersects the particle randomly in the case of intergranular fracture. This is not the same as saying that the fracture is a random fracture; it is only random as far as the particle is concerned (Fig. 4).

3.7. Estimation of the volume fraction of cavities in the plastically deformed zone

A study of the cavities, which form (or are there already) in the plastic zone and which surround the fracture surface, is necessary to understand fracture. El Soudani [7] has derived various expressions to calculate the volume fraction of voids or cavities for the majority of cases which are likely to arise.

Fig. 5 shows a fracture zone containing voids and explains the significance of the various parameters used by El Soudani [7]. To facilitate the calculations he considered that the plastic zone is limited by two parallel planes one on each side of the fracture. Inside this zone he defines a volume for analysis by a further two planes, parallel to the original planes and located into the plastic zone.

Several situations can arise:

(1) the cavities are all within the zone of analysis and no voids are truncated. In the opposite situation some cavities are truncated.

(2) all the cavities are truncated by the line of fracture, and there are no hidden cavities. If not all cavities are truncated, some will remain undetected.

It is possible to present the various possibilities making the general hypothesis that the cavities, when cut by the fracture, are cut through their centre, i.e. their largest diameter.

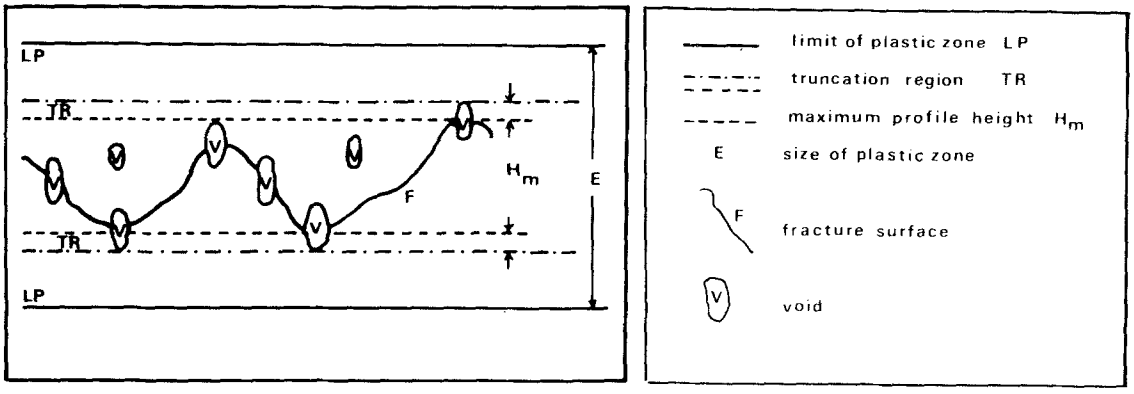

Figure 5 Schematic representation of a fracture encountering cavities in the zone of plastic deformation in the vicinity of the fracture, after El Soudani.

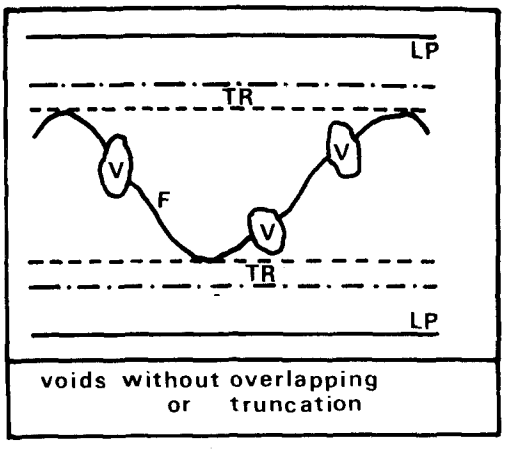

Figure 6 Fracture without truncated cavities and without undetected cavities.

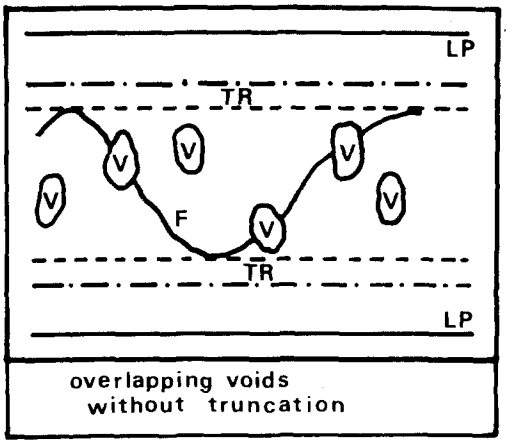

Figure 7 Fracture without truncated cavities and with undetected cavities.

3.7.1. Case in which no cavity is truncated and no cavity remains undetected

In this case the volume fraction has a value (Fig. 6).

$$V_V(\text{cavity}) = \frac{S_S(\text{cavity})\,\bar{L}_3\,(\text{cavity})}{E} \quad (14)$$

where

E is the thickness of the plastic zone,
H is the maximum distance of the tangent planes to the fracture surface, parallel to the mean fracture direction.

This equation is applicable in cases of slow crack propagation and low volume fraction of cavities.

3.7.2. Case in which cavities are not truncated but remain hidden

In this case (Fig. 7):

$$V_V = \frac{S_S \bar{L}_3}{2\bar{H}} \quad (15)$$

This equation is applicable in the case of unstable fracture and a large volume fraction of cavities.

3.7.3. Case in which cavities are truncated but do not remain hidden

In this case (Fig. 8):

$$V_V = \frac{S_S \bar{L}_3}{\bar{L}_3 + E} \quad (16)$$

This equation is applicable in the case of mean rates of crack propagation, as for example in steels or aluminium alloys, and in the case of cavities volumic fractions up to about 10%.

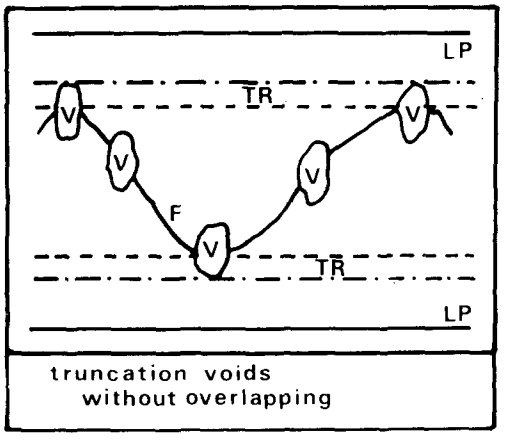

Figure 8 Fracture with truncated cavities and without undetected cavities.

3.7.4. Case in which there are both truncated and undetected cavities

In this case (Fig. 9):

$$V_V = \frac{\bar{L}_3 S_S}{\bar{L}_3 + E} \times \frac{S_V(\text{total})}{S_V(\text{fracture})}. \quad (17)$$

All these expressions have been derived without making any other hypothesis than that the cavities are convex and they are intersected by the fracture plane, if it exists, as in the analysis of thin films.

Note that the volume fraction can only be calculated if assumptions are made as to the shape of the cavities. In effect, if the quantity E can be obtained from the fracture mechanics data, then $\bar{L}_3$ and H can only be obtained by making assumptions as to the shape of the cavities. To assume that the cavities are spherical would be an over-simplification since the majority of fractographic

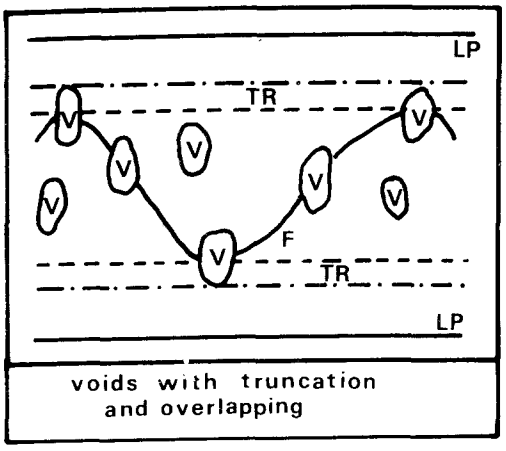

Figure 9 Fracture with truncated cavities and with undetected cavities.

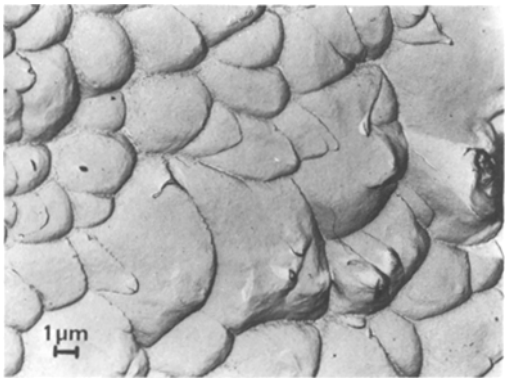

Figure 10 Fractography of a ductile fracture in an alloy TA6V.

studies of ductile failure show the cavities to be ellipsoids. Furthermore the prolate spheroids are elongated rather than flattened (Fig. 10).

For such cavities, if the eccentricity of these ellipsoids is known, it is possible to calculate $\bar{L}_3$. If a is the major axis and b the minor, the volume of the ellipsoid is:

$$V = \tfrac{4}{3}\pi a^2 b. \tag{18}$$

The surface area of the ellipsoid is:

$$S = 2\pi b^2 + 2\pi \frac{ab}{\epsilon} \sin^{-1} \epsilon \tag{19}$$

where ϵ is the eccentricity.
Since $\bar{L}_3$ is related to the surface area and volume of a body by Equation 3, one can write:

$$\bar{L}_3 = \frac{4V}{S} \tag{20}$$

Combining Equations 18, 19 and 20, and assuming the ellipsoids to have effectively the same eccentricity and size, one obtains:

$$\bar{L}_3 = \frac{8}{3} \frac{1-b^2}{b^2\epsilon^2 + b \sin^{-1} \epsilon \sqrt{(1-b^2)}} \tag{21}$$

$\bar{b}$ should be known as it is the mean diameter of circle obtained by intersection of the ellipsoid with the fracture surface.

It should be noted that it is possible to determine the volume fraction of cavities in the plastic zone by assuming that the fracture path passes randomly through randomly distributed and oriented cavities (for example the case of rapid crack propagation [7]):

$$V_V = S_S \tag{22}$$

4. Problems in linear analysis of fracture

Linear analysis of fracture can provide information which often complements that obtained from an analysis of the surface. This analysis is facilitated if the fractured specimens possess plane faces. It is obvious, however, that the fracture lines apply only to a particular stress state as only the external surface is investigated.

4.1. Measurable parameters

An analysis of the line of fracture is made essentially by linear analysis techniques. All the parameters measurable in a linear analysis on a section can be measured if the specimen surface is flat (Fig. 11). For example, the proportion of an object, seen by the line of fracture, L_L, can be calculated, and then the numbers of objects per unit length, N_L, and the size distribution of the objects. It is necessary, however, to realize that the meaning of the parameters depends on the type of fracture. The various possible situations are: either fracture occurs via the objects considered (for example brittle fracture by cleavage, ductile fracture of a matrix, etc.) or fracture circumvents the objects to be analysed (for example intergranular fracture, etc.). When fracture occurs through the objects to be analysed, there is no hypothesis which can be made to determine the derived parameters. On the other hand, when fracture occurs avoiding the objects, the definitions of some parameters can be modified (Table IV).

As for the proportion of the objects revealed by the fracture line, the expression for fracture by decohesion can be applied. The same applies for the expression for the number of objects per unit

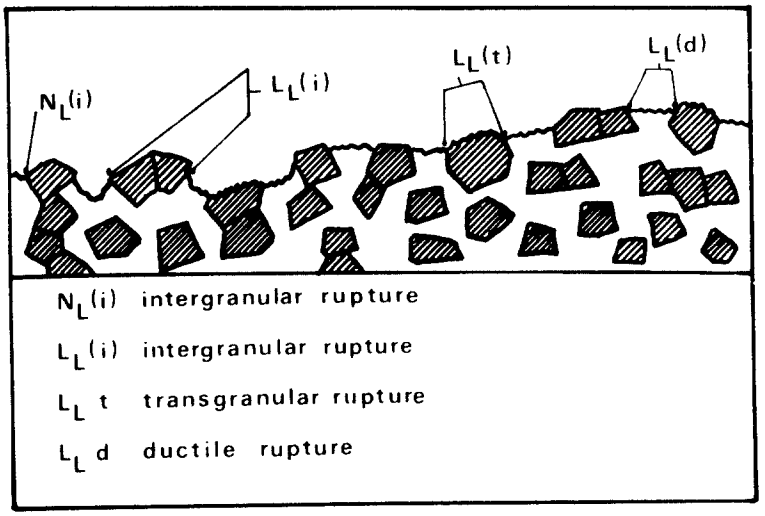

Figure 11 Parameters measured on the fracture line.

TABLE IV Specific parameters for a fracture line

L_L	Fraction of line occupied by a phase or type of fracture (transgranular, intergranular, ductile, etc.)
N_L	Number of objects per unit length (phase, type of fracture, grains, etc.)
L_1	Average size of objects intersected by the fracture line.
Relation	$L_1 = L_L/N_L$

length. On the other hand the parameter L_2, calculated from N_L in the analysis of sections, no longer has the same meaning. It no longer represents the mean chord obtained by intersection of a line with an object, but instead the mean length of perimeter of the object revealed by the fracture. To avoid confusion with L_2 we use another letter, $L_P(f)$. For the same reasons, it is impossible in intergranular fracture to measure the size distribution of particles revealed, using linear analysis. It is necessary, for this, to carry out measurements on the fracture surface itself. On the other hand, in transgranular fracture, the grain size distribution cannot be obtained from a surface analysis but solely by a linear analysis: only a part of the particle is visible, and the area below the polished surface where the fracture surface emerges is not known. For random fractures up to the surface Pickens and Gurland [12] have shown that $L_S = S_S$, and, hence, it is possible to deduce the behaviour over the whole surface from a study of the fracture path.

4.2. Analysis of the morphology of fracture

When the fracture line appears on a flat surface, its morphology can be analysed. The section of a fractured specimen exhibits, in the same manner, the profile of the fracture surface on the sectional plane. Hence it is possible to identify the type of fracture and thus, after quantitative analysis, classify the fracture according to the groups discussed above.

The quantitative aspects of this morphology are much more difficult to resolve, because one is confronted with the problem of the quantitative definition of the shapes. Shapes of objects can only be defined by comparison with geometric shapes defined previously. On the other hand the more or less wavy appearance of the fracture path can be expressed by a parameter. Several authors have already attempted a definition of the waviness. We shall first review these attempts and then propose a new definition.

Pickens and Gurland [12] proposed a linear roughness index, R_L, defined as the ratio of the true length of the fracture line to its projected length on a reference line. They noted that R_L depended on the orientation of the reference line. Hence for it be unequivocal the reference line must be chosen parallel to the mean fracture plane. These authors also noted that the apparent roughness is strongly affected by the magnification used and the resolution of the system. Chermant *et al.* [13] proposed a waviness index, P_S, which is the ratio of the length of the fracture line to the length joining the two extremes of the field being measured. This index is practically the same as R_L. It also depends on the magnification (Fig. 12).

These two parameters are easily measured, but provide little information as to the nature of the roughness.

It is possible to define the morphology of the

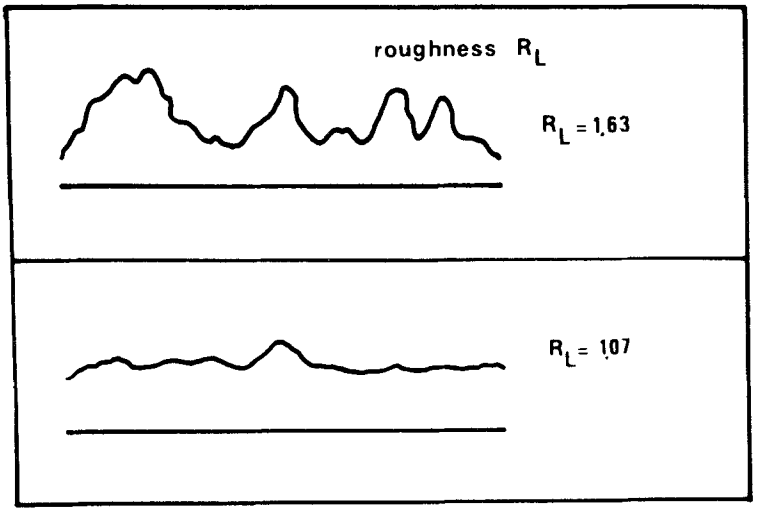

Figure 12 Waviness index.

TABLE V Morphological parameters for a fracture line

R_L	Linear roughness index
P_S	Waviness index
$\mathscr{D}$	Fractal dimension
$\bar{K}$	Absolute mean curvature
$\bar{K}^+$	Mean convex curvature
$\bar{K}^-$	Mean concave curvature
Relation	$R_L \simeq P_S$
	$\bar{K} = (\bar{K}^+ + \bar{K}^-)/2$

fracture line by its radius of curvature. One could attempt to calculate the mean radius of curvature, but in this case it is not possible to use the relationships proposed by Underwood [3], which assumed the lines to be positioned randomly on the surface being analysed. In our case the line follows more or less a preferred direction, and it is necessary to return to the definition of radius of curvature: $k = d\alpha/dl$, where α is the angle subtended by the line of length l. Pickens and Gurland [12] have shown that one could calculate the radius of curvature automatically by point-by-point analysis of the fracture line. This radius is equal to $k = 1/r$, where r is the radius of the circle passing by the extremities of the segment dl and centred on the middle of the segment. These authors then give the expression to obtain the mean radius of curvature:

$$\bar{K} = \frac{\sum_{i=1}^{n} K(i)}{n}. \quad (23)$$

In addition to this mean result, it is possible to calculate the distribution of radii of curvature, and also calculate separately the distribution of convex and concave radii of the fracture as shown in Table V.

Finally, we propose another definition of the roughness or waviness of the fracture line. The idea is to calculate the fractal dimension of the line of fracture. Since the concept of fractal dimension is not widespread it will be described in more detail.

There are a large number of objects which cannot be described by geometric figures as they are too irregular. Mandelbrot [11, 14] has shown that one could study these shapes using geometric concepts hitherto little used. He studied particularly irregular shapes, which were very irregular and more or less discontinuous: hence the term "fractal object".

The usually observed fracture line is more or less regular without any physical discontinuities, but with discontinuities in the geometric sense, i.e. points where the tangent to the fracture line is not defined. The fracture line falls within the scope of the conception of "fractal object" given by Mandelbrot. To describe the fractal objects, he uses the concept of fractal dimension. As a matter of fact there are several definitions of the dimension. The best known is the topological dimension. But to define the fractal dimension Mandelbrot has chosen the contents dimension of Hausdorff–Besicovitch [15]. An object will be called a fractal object if its contents dimension is always higher than its topological dimension. Unfortunately in image analysis the contents dimension is not accessible. An other concept of fractal dimension will therefore be chosen: the covering dimension [16]. There are several methods to reach the covering dimension. We shall describe the two simplest methods which can be used.

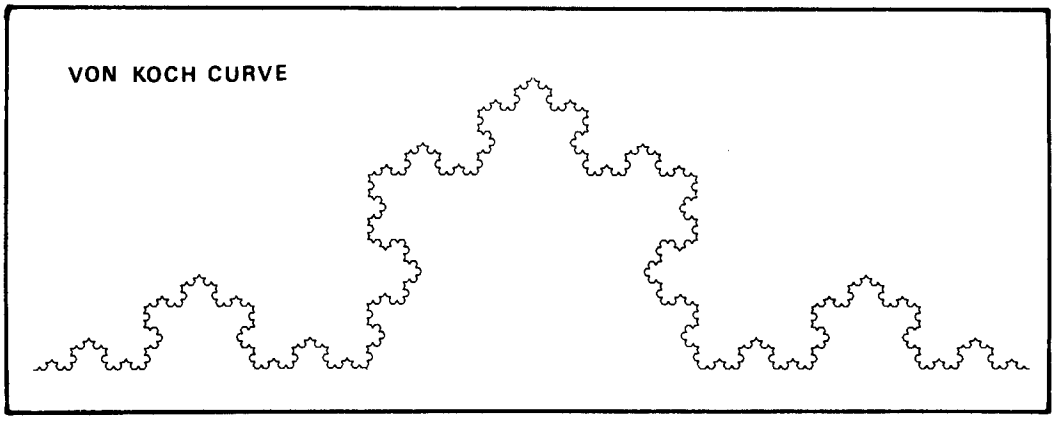

Figure 13 Von Koch curve.

4.2.1. First method

Consider a line, more or less irregular, describing a fracture line (Fig. 13), and then measure the length of this line, using a finite measurement step. The value so obtained is an approximate length, and increases if the step size is decreased. A large step erodes the majority of the angular fluctuations of the line. The measured length is then plotted double logarithmically against the step size. If, for a given step size, the curve is linear (Fig. 14), the fractal dimension of the line $\mathscr{D}$ can be calculated from the expression:

$$\log (L_{P_\alpha}) = (1 - \mathscr{D}) \log h \qquad (24)$$

where h is the measurement step size, and $(1 - \mathscr{D})$ is the slope.

This method has been used by Richardson to follow the evolution of the length of the terrestrial coasts, and Mandelbrot [14] showed that this method allows to reach the fractal dimension of a line. This method correspond to the determination of the contents dimension [16], and can be used with a digitalization table [17].

4.2.2. Second method

As for this second method, the contents dimension of Minkowski is determined in substituting the initial fracture line by a tape $2r$ thick. This process is similar to the process of dilation by a circle. In order to calculate the approximate length of this tape you have to measure the perimeter of the line enclosed by a circular structuring element.

We have shown that this method can be used with an automatic analyser using an iterative algorithm based on the principles of the mathematical morphology [18], provided that a process of skeletonization was carried out on the closed line [19].

For a fracture line, the fractal dimension lies between 1 and 2. The value is 1 for regular curves, with a defined tangent at all points. The value

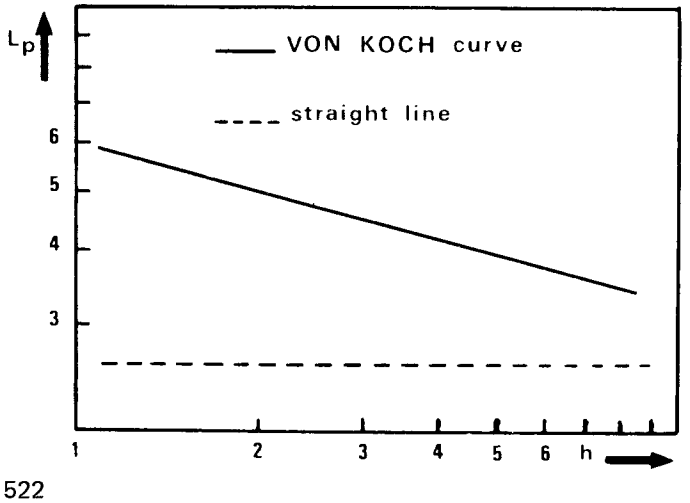

Figure 14 Curves of $\log \bar{L}_P = f(\log h)$, for a Von Koch curve and a straight line.

tends to 2 when the line fills all the space in the plane. The double logarithmic plot is linear if, for the range of step sizes chosen, the fracture line can be derivated by internal similarity, i.e. if, on changing from a large magnification to a smaller one, similar features are observed but on a smaller scale. This is always the case for the majority of natural seacoast lines, but not so for all fracture lines. If the curve is essentially linear for three scale magnifications, then it can be said that for a fracture for which the fractal dimension is not constant over most of its length, that this is due to one or at the most two physical phenomena. Thus for pure intergranular fracture, as shown in Fig. 15, the double logarithmic plot, shown in Fig. 16, is obtained. It is not truly

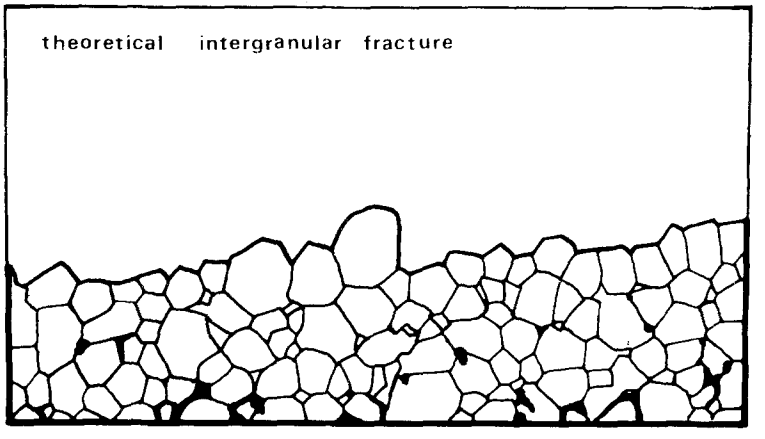

Figure 15 Theoretical intergranular fracture.

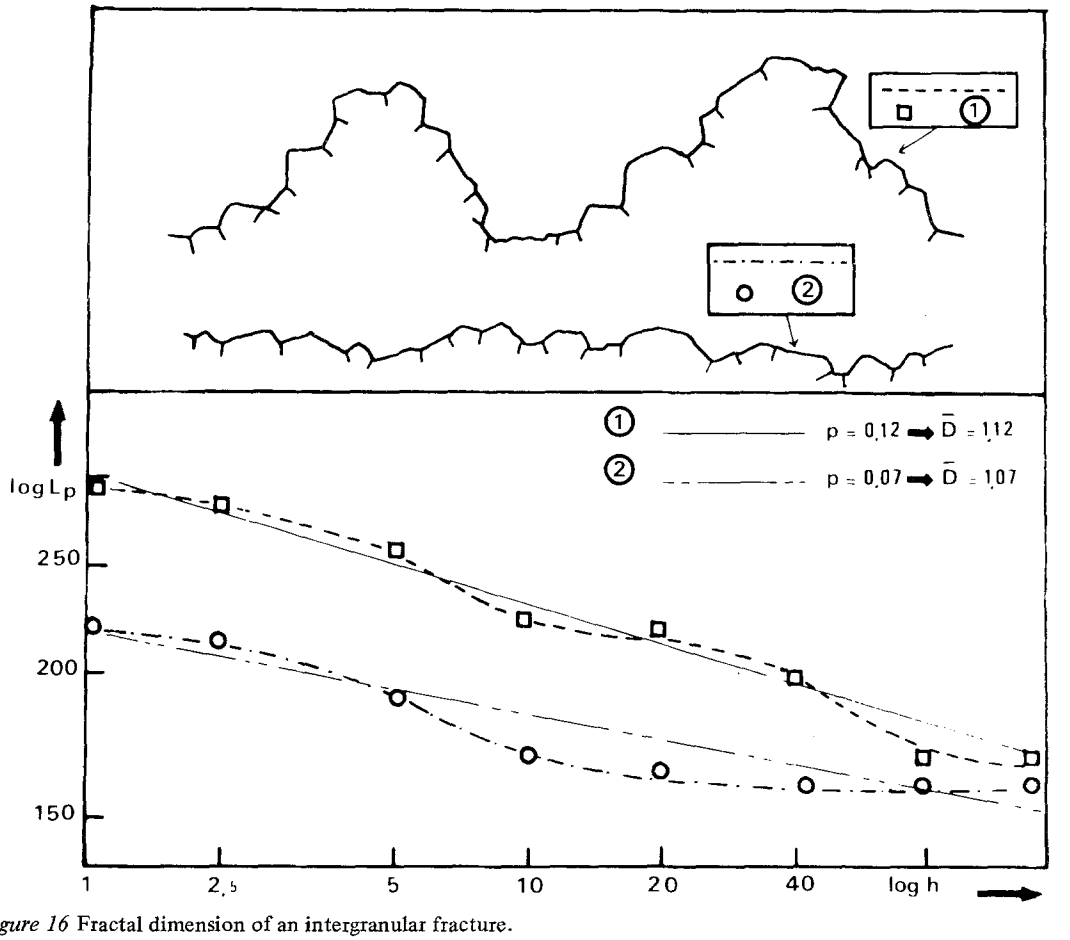

Figure 16 Fractal dimension of an intergranular fracture.

linear. This is due solely to the line of grain boundaries followed by the fracture.

Even if the fractal dimension of a fracture cannot be defined, because too few phenomena are responsible for its irregularity, it is still interesting to have the double logarithmic plot, because the slope, at a given point, is a function of the irregularity of the fracture line for the chosen scale. We have shown [18] that it is better to use the evolution of the linear roughness than the evolution of the perimeter. We have also shown that the derived curve:

$$\frac{\mathrm{d}\log(R_L)}{\mathrm{d}\log(h)} = f\log(h)$$

is similar to a spectrum the peaks of which correspond to the size of the phenomena responsible of the irregularity.

It can be said that this method produces a large amount of information on the rupture, and that, if the morphology of the bulk material is known, it is possible to explain much better the rupture mechanism of materials.

5. Comparison parameters

In the previous paragraphs we have shown that the same parameters can be measured either on the fracture surface, or on the fracture line. The different morphological parameters measured or calculated are not only interesting in themselves, as a direct comparison with the values measured or calculated from a polished surface, but also provide information leading to a better understanding of the fracture mechanism. It is for this reason that we have defined comparison parameters to underline the differences between the plane section and the line or the fracture surface. It is not the intention to present an exhaustive list, but rather to show how these parameters are chosen and used.

To define a discrepancy parameter, which has real significance, it is necessary that the parameters measured on the polished surface and the fractured surface have the same meaning, and obviously are of the same type. For example, one can calculate the discrepancy between the amount of a phase on the fractured surface and the polished surface, whereas the proportion of transgranular fracture, which is measured in the same way as the ratio of a phase on the fracture surface, cannot lead to any discrepancy parameter since there is no equivalent measurement on the polished surface. The first discrepancy parameter, we used, was just the discrepancy, Δ, between the proportion of a phase on the fracture surface and the polished surface [13]:

$$\Delta(A_A) = \frac{A_A(\text{fracture surface})}{A_A(\text{polished surface})} - 1 \quad (25)$$

For the other mean specific parameters, measured equally well on the fracture surface as on a section, it is preferable to use their ratio as comparison parameter. Thus one can define:

$$\rho(N_L) = \frac{N_L(\text{rupture})}{N_L(\text{polished surface})} \quad (26)$$

where N_L can be the number of crystals per unit length, and:

$$\rho(N_A) = \frac{N_S(\text{rupture})}{N_A(\text{polished surface})} \quad (27)$$

where N_A can be the number of crystals per unit surface area.

These various parameters have the following meanings:

(1) For Δ, a positive value shows that a phase appears preferentially on the fracture surface, the more so the larger is Δ. A negative value of Δ shows that the fracture avoids to a certain extent a particular phase.

(2) For ρ, a value less than 1 shows that fracture proceeds preferentially in the large crystals, and more so the smaller is ρ. A value greater than 1 indicates the opposite effect.

The discrepancy parameters defined above are derived from mean specific parameters. It is equally possible to establish comparison parameters from granulometric data obtained on polished and fractured surfaces [20].

Consider, for example, a granulometric analysis of fractured crystals on a fracture surface and the same two-dimensional analysis on a polished surface. To obtain a discrepancy parameter between the measurements, we cannot use the frequencies but only the granulometries calculated in number of crystals per unit area, if the comparison is to have any significance. Then the ratio of the granulometries calculated in number of crystals per unit area, if the comparison is to have any significance. Then the ratio of the granulometries provides a probability curve for fracture (Fig. 17). We define as comparison parameter the critical diameter, D_C, which is the size of crystals with a

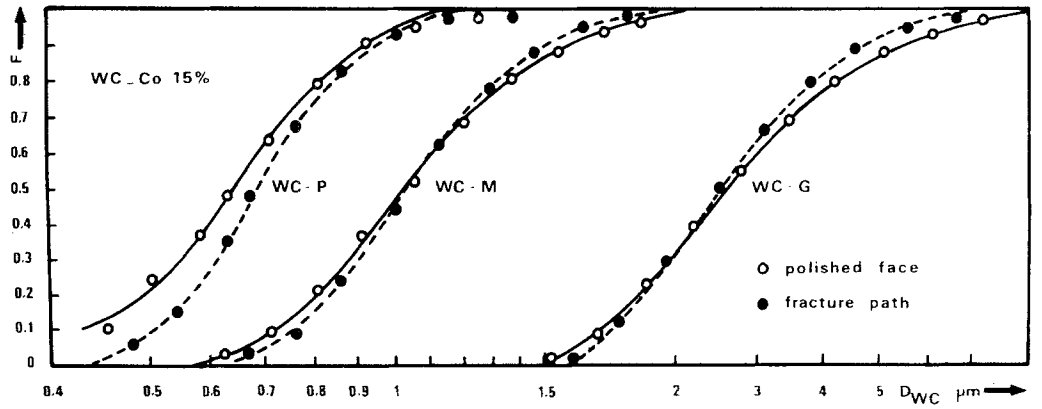

Figure 17 Distribution curves of WC crystals on fractured and polished WC–15 wt % Co specimens.

probability of fracture of 0.5. The choice of this value is justified by the fact that the probability curve varies rather rapidly for this value. The parameter D_C can thus be calculated reasonably accurately, which would not be the case if one had taken a value for the probability of 1. In this case the granulometry can be expressed as the diameter of equivalent spheres using the Saltykov method, modified for granulometry in surface [20].

6. Mathematical morphology and quantitative fractography

We shall discuss here briefly the contribution which mathematical morphology can make to quantitative fractography.

6.1. Properties of variograms and covariograms

In the majority of cases, quantitative analysis of a fracture surface using classical method is sufficient to describe the fracture morphology. However, no parameter hitherto employed is capable of describing the periodicity of a phenomenon, or of describing phenomena which occur at different magnifications. Thus one can find, in a fracture, a surface zone of principally transgranular fracture followed by zones of principally intergranular fracture. With this example, it is possible to utilize the properties of the variograms of the regionalized function (for example S_S(intergranular)) in introducing, into regular space, the fields of measurements, and then measuring in each field the proportion of intergranular fracture.

The regionalized covariogram is calculated from the expression [4, 5]:

$$\gamma(h) = \mathscr{E}\{[S_S(x+h) - S_S(x)]^2\} \quad (28)$$

The derivative at the origin of such a variogram [21] is equal to the number of times one can penetrate the favoured zone for intergranular fracture per unit length, $\bar{N}_L$ (intergranular zone). The mean size in the direction of analysis of these zones is thus:

$$\bar{L}_2(\text{intergranular zone}) = \frac{\bar{S}_S(\text{intergranular})}{\bar{N}_L(\text{intergranular zone})} \quad (29)$$

The measurement step h of such a variogram is to be corrected from equations in Table III giving L as a function of the type of fracture encountered; for example for a random fracture:

$$h = \frac{4}{\pi} h', \quad (30)$$

where h' is the projection of the step h on to the plane of analysis.

The appearance of the variogram away from the origin shows that there are periodic phenomena of drift of the specific parameter in the direction of analysis (Figs. 18 and 19).

The example to be presented is not the only possibility of the variogram: it may be used with other specific parameters in the case where these other quantities are characteristics of the investigated regionalization.

The covariogram is derived from the variogram. Often a particular covariogram is used in mathematical morphology, the geometric covariogram, as well as its probabilistic aspect, the covariance function $C(h)$, [6, 22]. This function, of which the support is the point, is a function of everything or nothing. It corresponds to the probability of two points, separated by h, falling in the same

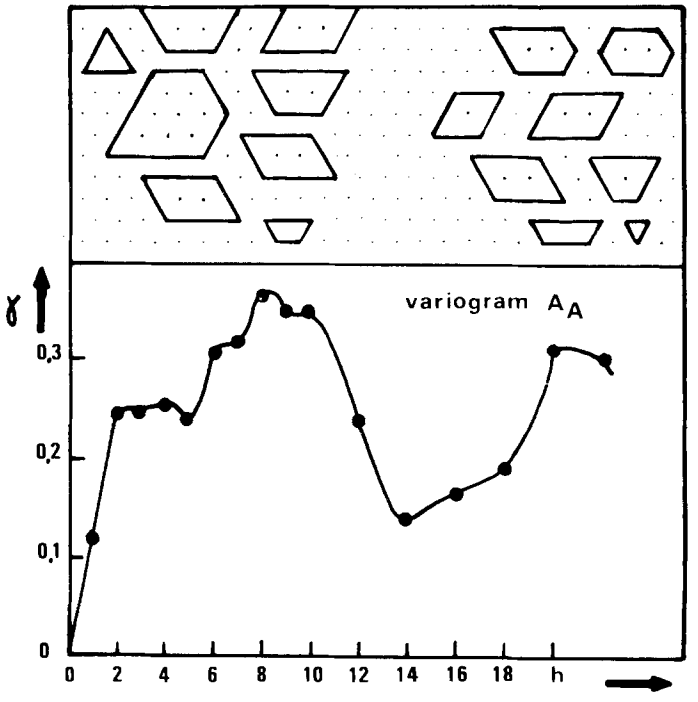

Figure 18 Variogram of a pseudoperiodic structure.

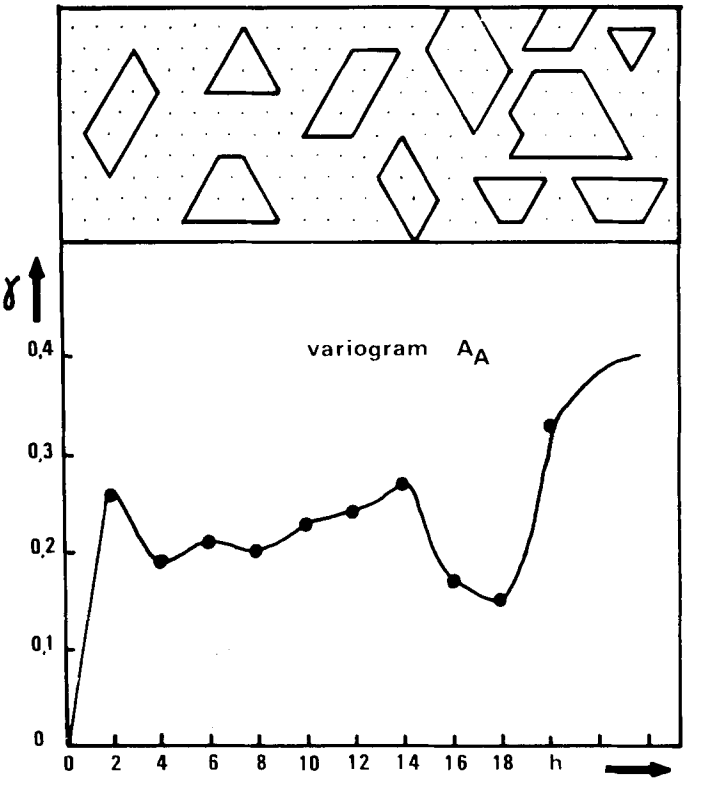

Figure 19 Variogram with drift of the amount of crystals.

phase. This function is sensitive to the anisotropy of the surroundings. As are all measurements using linear analysis, it contains information on the imbrication of the phases and on the periodic phenomena. In the case of quantitative fractography the measurements made on the phases can be extended to measurements on the features, considering each feature as an entity. The same type of corrections used for the variogram must be used for the step h in the covariance function.

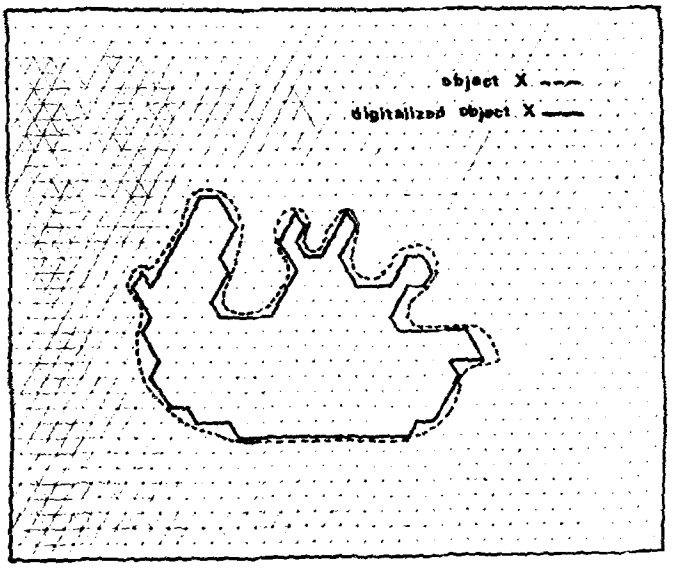

Figure 20 Digitalized object with a hexagonal frame.

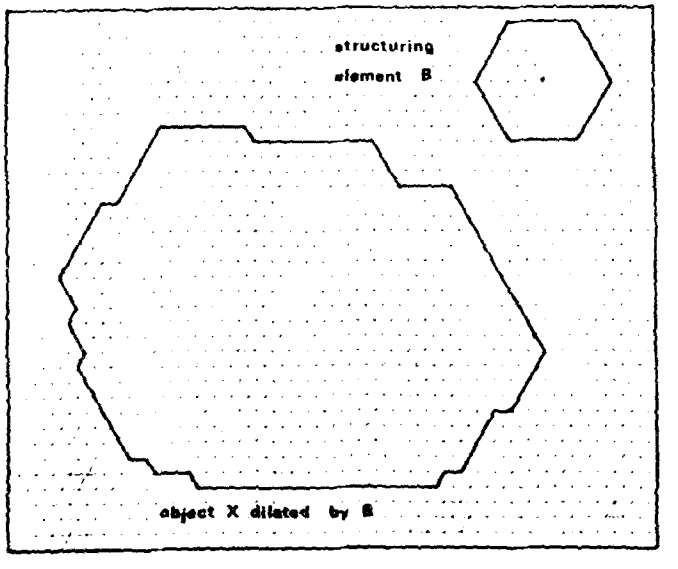

Figure 21 Dilation of the object of Fig. 20.

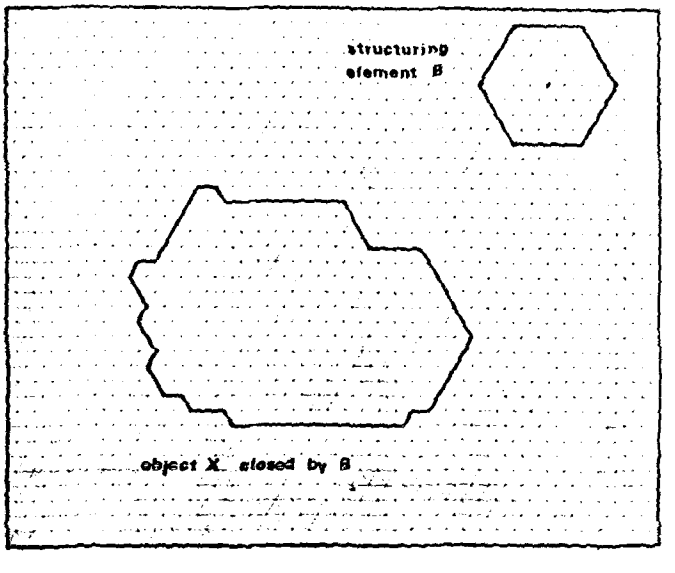

Figure 22 Closing of the object of Fig. 20 (eroding of the dilated object).

6.2. Closing of a fracture by a hexagonal structuring element

Another possibility of using mathematical morphology to describe fracture consists in closing the fracture line by a hexagonal structuring element. This operation has already been described in the publications of Matheron [4] and Serra [6]. The closing by a two-dimensional structural element of the object X to be analysed, followed by the eroding operation of the dilated object by the same structuring element, which is expressed by:

$$X^{B(r)} = [X \oplus B(r)] \ominus B(r) \qquad (31)$$

where $B(r)$ is the structuring element.

The Figs. 20, 21 and 22 show the result of such a morphological transformation. It can be seen that the irregularities in Fig. 20 disappear after the closing operation. If the perimeter of such a shape is determined, before and after the closing operation, it can be seen that the length is much smaller after closing and that the perimeter decreases for increasing structuring elements (in this case hexagonal). By studying the closing operation for increasing sizes of structuring elements, which measures the perimeters of the transformed object, it is possible to establish the relationship (apparent perimeter) $= f$(log step of structuring element). This leads to the determination of the fractal dimension of the object under consideration using a method of covering by a geometrical shape which is the structuring element [18].

7. Available methods of measurement

Generally the methods of image analysis can be subdivided into three groups:

(1) manual analysis,
(2) semi-automatic analysis,
(3) automatic analysis.

7.1. Manual analysis

Manual analysis can be point, line or area, depending on the specific quantity being investigated. It can be carried out, irrespective of the method of observation used, as soon as the image can be resolved by the human eye. It is a method which can be applied equally well to scanning electron microscope images or transmission electron microscope on replica. Manual methods can be used equally well to analyse a fracture line observed in the optical or scanning electron microscope. Unfortunately, although this is cheap, it is long and tedious, particularly to establish the size distribution of particles. It cannot be applied to obtain the covariance or measure the fractal dimension of a fracture line.

Generally to measure A'_A or S_S, experience has shown that it is preferable to use a point method rather than a linear method [8]. Surface analysis is used only to count the number of objects. The majority of fractographic studies, undertaken to the present time, have used manual methods.

7.2. Semi-automatic analysis

The Zeiss TGZ 3 is a semi-automatic analyser, and can be used to determine the size distribution of particles, as the diameter of equivalent circles, by comparing the grain size with an illuminated variable size spot. It is well suited to this type of measurement, since the actual comparison is made by eye. The choice of an arithmetic or geometric classification is a further advantage since, for example, with a geometric progression of the class sizes it is possible to use the Saltykov correction [1, 23].

For all other measurements there are numerous digitalizers on the market which enables data assessed by eye on the object table, to be fed automatically into a small computer. With a suitable program the desired specific parameters can be evaluated [17]. There is one such table on the market coupled to a microprocessor and which provides characteristic parameters directly (Leitz, ASM Table) [24]. Such tables can be used also to obtain the fractal dimension of the fracture line using the Richardson method [14, 18], and also to calculate all the morphological characteristics of the fracture line.

7.3. Automatic analysis

It is not possible at the present time to analyse a fracture and determine specific parameters with the automatic analysers commercially available. The detection of various objects and their discrimination is only possible if each family has the same degree of greyness, which is not the case in fractographic images.

It is only possible to use the automatic analyser to determine the fractal dimension of a fracture line [18] when the analyser is or can be equipped to undertake the closing operation of a two-dimensional structuring element (for example with a Leitz TAS or a Cambridge Instrument QTM 720).

There now exists a prototype model of an

instrument called AT IV, devised by the Centre de Morphlogie Mathématique de Fontainebleau. With this automatic analyser it is possible to analyse complex images, after a point-by-point memorization of the detected image [25, 26].

8. Examples of applications

As the conclusion of this study, and to show that quantitative fractography is an excellent experimental technique, we shall give some examples of its applications in solving certain practical problems and even to explain completely the mechanisms of fracture.

In essence we have known for some time the relationships which exist between microstructural parameters and mechanical characteristics, as for example the Hall–Petch relationship. These laws are applicable particularly to plastic deformation. Complementary information on fracture is necessary to establish the fracture mechanism with any degree of certainty.

8.1. Structure and fractography of WC–Co

One of the first articles to show an application of quantitative fractography was that of Mason and Kenny [27]. In this article the authors measured first the microstructural parameters describing the microstructure of bulk tungsten carbide–cobalt materials, for example $N_L(WC)$, $N_A(WC)$, the distribution of the chord lengths using the method of Lord and Willis [28]. Other authors have measured for the same materials the mean free path in the cobalt phase and the contiguity of the carbide phase [29]. In this type of material, three types of fracture are encountered: a ductile fracture in the cobalt phase; a transgranular fracture in the carbide phase; and an intergranular fracture between neighbouring WC–WC crystals. The fracture had been caused by Vickers hardness tests. Mason and Kenny found that the proportion of transgranular fraction follows a law:

$$\log A_A(\text{transgranular}) = \frac{4K[1 - V_V(\text{Co})]}{D}$$

$$(\text{with } K = Ct).$$

They also found that the proportion of intergranular fracture was largest and that the proportion of fracture in the cobalt increases with the volume fraction of cobalt. They explain these results as follows: transgranular fracture occurs when intergranular fracture is less probable (presence of large crystals). The increase of ductile fracture in the cobalt with cobalt composition is due to the local values of the modulus of elasticity and to the stress field in the cobalt zones.

8.2. Behaviour of MC–Me composites under high pressure

We have determined the principal mechanical characteristics on the same types of material and related the characteristics to morphlogical changes as a result of mechanical tests. For example, we have studied the behaviour under high pressure (40 to 120 kbar) of metal–carbide composites. WC–Co [30] composites were studied first, and then the tests repeated for other composites including TiC–Co and TiC–Ni [20, 31]. We observed that pressure induces slip in the WC crystals. The degree of slip is greatest for large

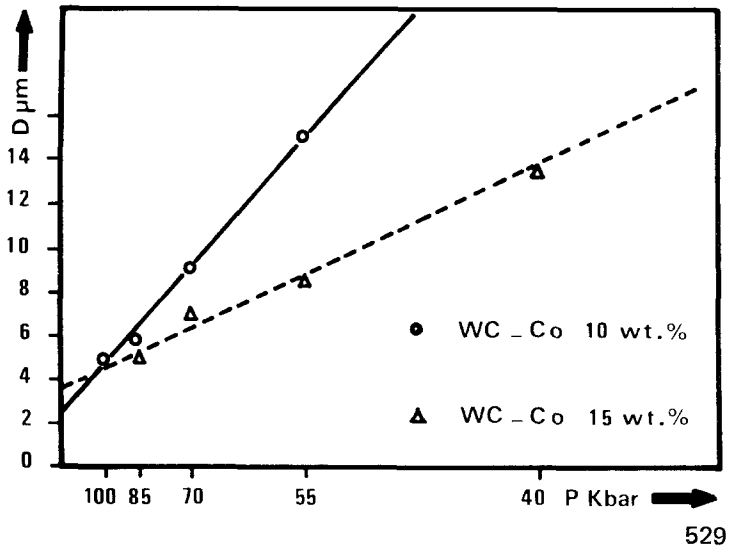

Figure 23 Variation of the critical diameter of slip as a function of the applied pressure for different WC–Co materials.

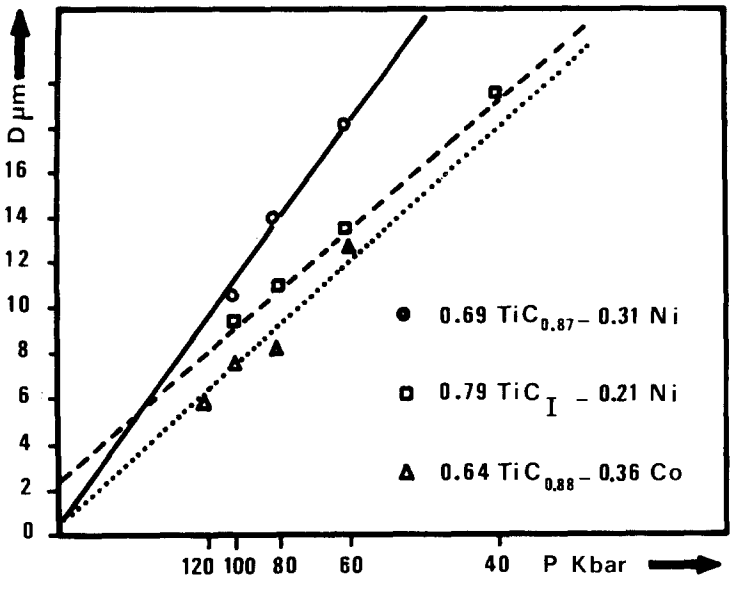

Figure 24 Variation of the critical diameter of fracture as a function of the applied pressure for different TiC–Co and TiC–Ni materials.

crystals and high pressures. Using the TGZ 3 semi-automatic analyser, we measured the size distribution on the surface of carbide crystals exhibiting slip and calculated the distribution N_V as the diameter of equivalent spheres, with the modified Saltykov method. This size distribution of slipped WC crystals has been compared to that in the bulk material. The ratio of the two distributions gives the probability of slip and the critical diameter of slip, as defined above. We have thus been able to establish a law of the type (Fig. 23):

$$D_c = K'P^{-1} + B$$

where P is the applied pressure and D_c the critical diameter.

In the case of TiC–Co and TiC–Ni, the same procedure was followed, but these materials are more brittle. The carbide crystals fracture under the influence of pressure. We have thus established, for this case, a critical diameter of fracture which leads to a law of the type (Fig. 24):

$$D_c = K'P^{-1} + B$$

8.3. Behaviour in bending of WC–Co

Similar quantitative analysis were carried out in a study of the behaviour of WC–Co composites [32, 33] subjected to bending or toughness tests.

Initially the size distribution of particles was determined for the bulk material, then for the crystals observed on the fracture on a scanning

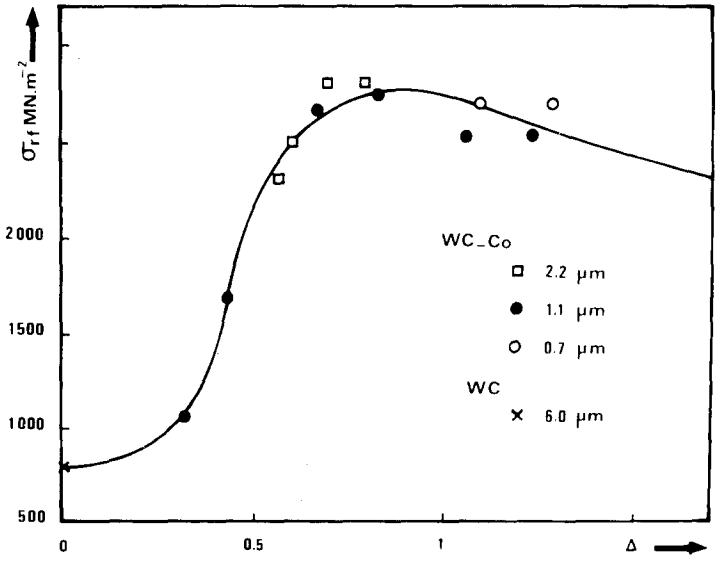

Figure 25 Variation of the rupture stress in bending, σ_{rf}, as a function of the discrepancy parameter, Δ, for WC–Co materials.

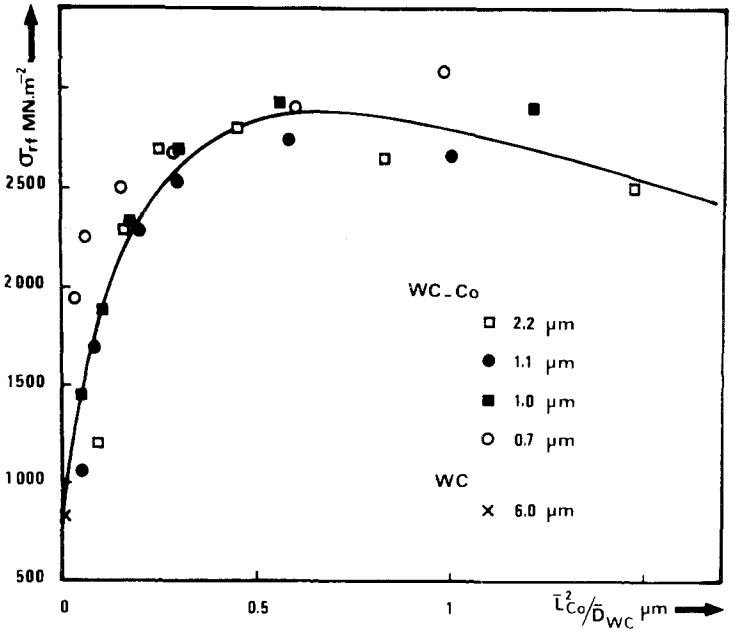

Figure 26 Variation of the rupture stress in bending, σ_{rf}, as a function of $\bar{L}^2_{Co}/\bar{D}_{WC}$ for different WC–Co materials. ($\bar{L}_{Co}$, mean free path in the cobalt phase; $\bar{D}_{WC}$, mean diameter of the tungsten carbide crystals).

electron microscope image [32]. The curves obtained for the different materials show that there are fewer smaller crystals on a fracture surface than on a random section. A more complete study was undertaken, using different methods to determine the proportion of cobalt on the fracture surface (X-rays image, secondary electron) [8, 9]. From a comparison of the various values obtained, it was obvious that the proportion of cobalt on the surface was greater than the volume fraction, but this increase is due principally to a thin layer of cobalt (X-rays image (W)). This difference in proportion of cobalt has been studied as a function of WC–Co composition, for different bend specimens, using the discrepancy parameter, Δ, described above [13]. The change of this discrepancy parameter was studied for un-notched specimens as function of the fracture stress (Fig. 25) and the rupture stress as a function of the microstructural parameter $\bar{L}^2_{Co}/\bar{D}_{WC}$ (this parameter is the ratio of the square of the mean free path in the cobalt phase, $\bar{L}_{Co}$, to the mean diameter of WC crystals, $\bar{D}_{WC}$) (Fig. 26). The following conclusions can be drawn from the two curves:

(1) The parameter $\bar{L}^2_{Co}/\bar{D}_{WC}$ is a parameter which describes unambiguously the mechanical behaviour of different WC–Co grades.

(2) The change of Δ as function of σ_r shows

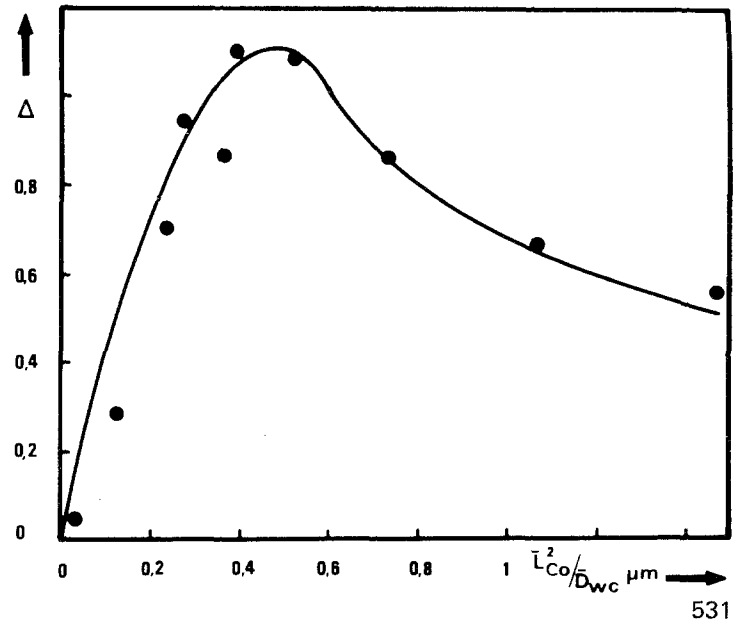

Figure 27 Variation of the discrepancy parameter, Δ, as a function of $\bar{L}^2_{Co}/\bar{D}_{WC}$ for different WC–Co materials. ($\bar{L}_{Co}$, mean free path in the cobalt phase; $\bar{D}_{WC}$, mean diameter of the tungsten carbide crystals).

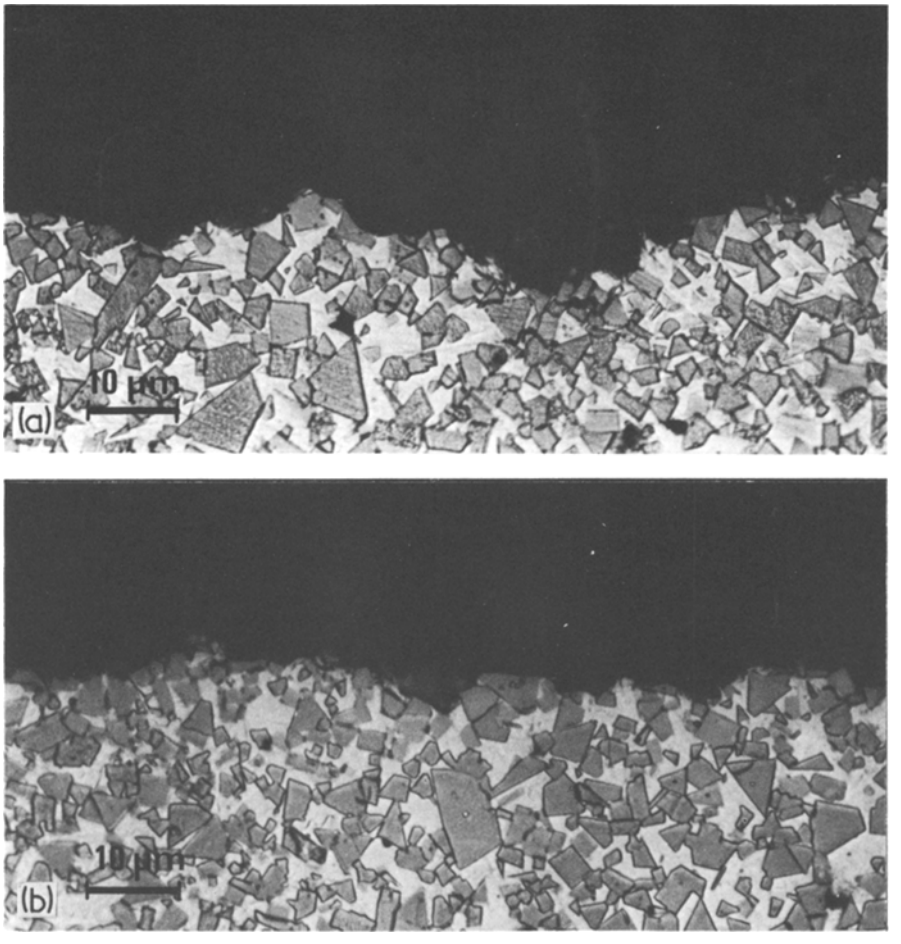

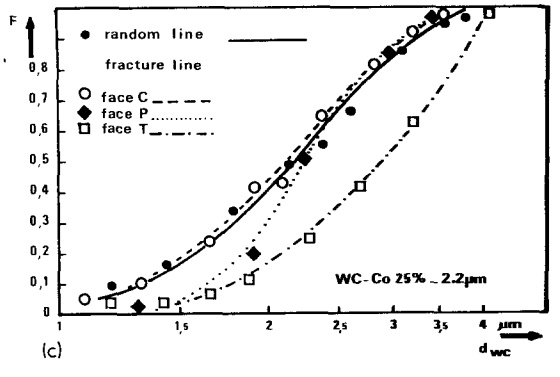

Figure 28 (a) Micrographs of fracture lines on WC–Co (25 wt%, $\bar{D}_{WC} = 2.2\,\mu m$) bend specimen, on the tensile polished face; (b) on the compression polished face. (c) Distribution curves of the WC crystals for WC–Co specimen (25 wt%, $\bar{D}_{WC} = 2.2\,\mu m$) fractured in bending.

that the strongest materials are those for which fracture occurs predominantly in the cobalt phase, which occurs at a well-defined value of $\bar{L}^2_{Co}/\bar{D}_{WC}$ (Fig. 27).

The fracture line was analysed for these same materials, and the waviness index, as defined above, determined as well as the proportions of the various fracture types: L_L (transgranular), L_L (intergranular), and L_L (fracture in the cobalt). Using these results, we showed that the waviness of fracture increases with increasing cobalt content, and was greater for fracture in tension than in compression.

Furthermore the proportion of transgranular fracture is much higher in the outer surfaces. This may be explained by the fact that the crystals are more brittle here, due to the fact that the stresses are very asymmetric in the surface layers.

Fig. 28 shows the size distribution of crystals fractured on the various faces. It can be seen in particular, that it is the largest crystals which fracture most frequently. This effect is even more pronounced for a surface in tension, which confirms that it is at such faces that fracture is initiated in bending.

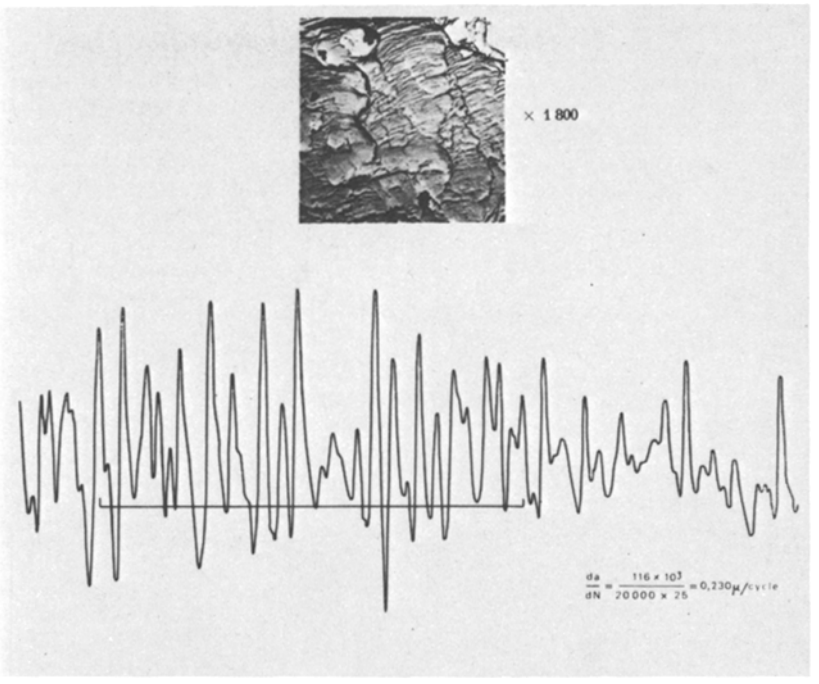

Figure 29 Registration of the number of striations with the microdensitometer for a ferritic steel, 0.9% C, after Bathias.

The same analysis was carried out on notched specimens in order to measure the critical stress intensity factor, K_{IC} [33]. It was found that fracture was principally intergranular and that the fraction of transgranular fracture exhibited a maximum for certain values of $\bar{L}^2_{Co}/\bar{D}_{WC}$. It was likewise shown that G_{IC} was a linear function of this combined parameter.

8.4. Fracture of the oriented lamellar eutectic $Ni/Ni_3Al–Ni_3Nb$

Some investigations have also been undertaken on the fracture of lamellar composites. Sheffler and co-workers [34] has shown recently that for eutectic lamellar $Ni/Ni_3Al–Ni_3Nb$ the fracture path cannot be described by one type of behaviour, although they did make a specific measurement of this. It would be interesting to relate the morphology of the fracture line to the microstructure, particularly because the microstructure can be established easily with an automatic texture analyser, Leitz TAS, as we have shown in the case of directionally white cast iron [35, 36].

8.5. Fatigue striations in ferritic and austenitic steel

As the last example of the application of image analysis to fractography, we have choosen the measurement of the size of fatigue striations. Bathias [37] has devised an automatic method of measuring the interval between the striations. He takes the photographic plates exposed in the electron microscope and analyses them with a microdensitometer equipped with a XY recorder. The striations are oriented perpendicular to the direction of plate displacement, so that when each striation passes the window of the reader, a peak is registered on the recorder (Fig. 29). The analysis of the diagrams enables the number of peaks to be counted and the interval measured.

9. Conclusion

The various aspects of fractographic analysis discussed together with various examples emphasize on the one hand what a powerful tool quantitative and stereological analysis is, and on the other hand the wide range of fields in which it can be applied.

Acknowledgements

We want to particularly thanks Professor B.L. Mordike for reading the manuscript critically and improving the English.

References

1. S. A. SALTYKOV, "Stereometric metallography" (Metallurgizdat, Moscow, 1958).
2. R. T. DE HOFF and F. N. RHINES, "Quantitative Microscopy" (McGraw Hill, New York 1968).

3. E. E. UNDERWOOD, "Quantitative Stereology" (Addison Wesley, New York, 1970).
4. G. MATHERON, "Eléments pour une théorie des milieux poreux" (Masson, Paris, 1967).
5. G. MATHERON, "Les variables régionalisées et leur estimation" (Masson, Paris, 1965).
6. J. SERRA, "Introduction à la morphologie mathématique", Les Cahiers du Centre de Morphologie Mathématique de Fontainebleau (ENSMP, 1969).
7. S. M. EL SOUDANI, *Metallography* 7 (1974) 271.
8. M. COSTER, Thèse d'Etat, Université de Caen (1974).
9. J. L. CHERMANT, M. COSTER and A. DESCHANVRES, *Metallography* 8 (1975) 271.
10. M. G. KENDALL and P. A. P. MORAN, "Geometrical Probability" (Charles Griffin, London, 1963 pp. 74, 115.
11. B. MANDELBROT, "Les objects fractals, forme, hasard, dimension" (Flammarion, Paris, 1975) Ch. II.
12. J. R. PICKENS and J. GURLAND, Fourth International Congress for Stereology, Gaithersburg, Maryland (NBS Special Publication, 1976) p. 269.
13. J. L. CHERMANT, M. COSTER and F. OSTERSTOCK, *Metallography* 9 (1976) 503.
14. B. MANDELBROT, *Science* **155** (1967) 636.
15. F. HAUSDORFF, *Mathematische Annal.* 79 (1919) 157.
16. M. COSTER and J. L. CHERMANT, International Symposium on Quantitative Metallography, edited by Associazione Italiana di Metallurgia, Milan (1978) p. 125.
17. M. COSTER, *Pract. Met.* (to be published).
18. M. COSTER and A. DESCHANVRES, *Pract. Met.* 8 (1978) 61.
19. C. LANTEUJOUL, *ibid.* 8 (1978) 40.
20. J. L. CHERMANT, M. COSTER, G. HAUTIER and P. SCHAUFELBERGER, *Powd. Met.* **17** (1974) 85.
21. J. SERRA and P. CAUWE, "Le variogramme", fascicule 3 in 15 fascicules de Morphologie Mathématique Appliquée (Ecole des Mines, Fontainebleau, 1975).
22. T. HERSANT, D. JEULIN and P. PARNIERE, "Notions de base de Morphologie Mathématique utilisées en métallographie quantitative", Rapport IRSID, St-Germain en Laye (1976) and *C.I.T.* 6 (1976) 1449.
23. J. L. CHERMANT and M. COSTER *Pract. Met.* **14** (1977) 521.
24. W. MULLER and H. WASMUND, Leitz Wetzlar Scientific and Technical Information **6** (1976) 316.
25. BREVET No. 75–21–925, appareil destiné à analyser au moins un milieu hétérogène bi- ou tridimensionnel.
26. J. C. KLEIN, Thèse de Docteur Ingénieur, Université de Nancy 1 (1976).
27. A. MASON and P. KENNY, *Metallurgia* (1970) 205.
28. G. W. LORD and T. F. WILLIS, *A.S.T.M. Bull.* **177** (1951) 56.
29. J. GURLAND, *Trans. AIME* **212** (1958) 452.
30. M. CONTRE, M. COSTER, A. DESCHANVRES and L. PONS, IInd European Symposium on Powder Metallurgy, Stuttgart (1968) and *Powder Met. Int.* 3 (1971) 33.
31. J. L. CHERMANT, M. COSTER and A. IOST, Eleventh Annual Meeting of the European High Pressure Research Group, London.
32. J. L. CHERMANT, M. COSTER, A. DESCHANVRES and A. IOST, 4th European Symposium on Powder Metallurgy, Grenoble (1975) paper no. 5–9.
33. J. L. CHERMANT and F. OSTERSTOCK, *J. Mater. Sci.* **11** (1976) 1939.
34. K. D. SHEFFLER, R. H. BARKALOW, A. YUEN and G. R. LEVERANT, *Met. Trans.* **8A** (1977) 83.
35. P. CAMARD, J. L. CHERMANT and M. COSTER, *Pract. Met.* 8 (1978) 126.
36. P. CAMARD, Thèse d'Ingénieur Docteur, Caen (1978).
37. C. BATHIAS, Thèse de Doctorat ès-Sciences, Poitiers (1972).

Received 12 June and accepted 19 July 1978.